Since January 2020 Elsevier has created a COVID-19 resource centre with free information in English and Mandarin on the novel coronavirus COVID-19. The COVID-19 resource centre is hosted on Elsevier Connect, the company's public news and information website.

Biochemical and Biophysical Research Communications 591 (2022) 118–123

Contents lists available at ScienceDirect

Biochemical and Biophysical Research Communications

journal homepage: www.elsevier.com/locate/ybbrc

Merbromin is a mixed-type inhibitor of 3-chyomotrypsin like protease of SARS-CoV-2

Junjie Chen [a, b, 1], Yaya Zhang [c, 1], Dequan Zeng [a, b, 1], Bingchang Zhang [c], Xiaohong Ye [a, b], Zhiping Zeng [a, b], Xiao-kun Zhang [a, b], Zhanxiang Wang [c, d, **], Hu Zhou [a, b, *]

[a] School of Pharmaceutical Sciences, Fujian Provincial Key Laboratory of Innovative Drug Target Research, Xiamen University, China
[b] High Throughput Drug Screening Platform of Xiamen University, China
[c] Department of Neurosurgery, Xiamen Key Laboratory of Brain Center, The First Affiliated Hospital of Xiamen University, China
[d] School of Medicine, Xiamen University, Xiamen, Fujian, 361102, China

ARTICLE INFO

Article history:
Received 9 December 2021
Accepted 27 December 2021
Available online 30 December 2021

Keywords:
3CLpro
Protease
High-throughput screening
Inhibitor
Merbromin
SARS-CoV-2

ABSTRACT

3-chyomotrypsin like protease (3CLpro) has been considered as a promising target for developing anti-SARS-CoV-2 drugs. Herein, about 6000 compounds were analyzed by high-throughput screening using enzyme activity model, and Merbromin, an antibacterial agent, was identified as a potent inhibitor of 3CLpro. Merbromin strongly inhibited the proteolytic activity of 3CLpro but not the other three proteases Proteinase K, Trypsin and Papain. Michaelis-Menten kinetic analysis showed that Merbromin was a mixed-type inhibitor of 3CLpro, due to its ability of increasing the K_M and decreasing the K_{cat} of 3CLpro. The binding assays and molecular docking suggested that 3CLpro possessed two binding sites for Merbromin. Consistently, Merbromin showed a weak binding to the other three proteases. Together, these findings demonstrated that Merbromin is a selective inhibitor of 3CLpro and provided a scaffold to design effective inhibitors of SARS-CoV-2.

1. Introduction

Coronavirus disease 2019 (COVID-19) is an acute viral pneumonia, which was caused by infection with the severe acute respiratory syndrome coronavirus 2 (SARS-CoV-2). Up till now, more than 293 million people were infected, and the number of the infection cases is still climbing fast. SARS-CoV-2 originally named 2019-nCoV was determined to be a new member of the coronavirus family [1]. Despite genetic differences among SARS-CoV-2, SARS-CoV, and Middle East Respiratory Syndrome coronavirus (MERS-CoV), these coronaviruses have conservative function proteins, such as 3-chyomotrypsin like protease (3CLpro, also known as M^{pro} or nsp5 protease) [2,3]. 3CLpro is essential for the maturation of PP1a and PP1ab during virus replication, enabling it as a valuable target for the development of anti-coronavirus drugs [4,5]. Many compounds have been found as potent inhibitors of 3CLpro [6], however, there are no specific and effective drugs targeting SARS-CoV-2's 3CLpro in clinical application for COVID-19 treatment so far.

3CLpro functions as a main protease responsible for the maturation of the viral nonstructural proteins (nsps) by cleaving the large polyprotein at 11 sites from nsp5 to nsp16. The junctions of those nsps show an extensive homology and provide a good recognition site for 3CLpro [7,8]. Accordingly, synthetized peptides based on the amino acid sequences of the junctions were used as the substrate to evaluate the hydrolytic activity of 3CLpro in vitro [9]. This enzymatic assay system has been successfully applied for the screening of inhibitors that block the cleavage function of 3CLpro [6,10]. In this study, an in vitro screening model based on proteolytic activity of 3CLpro was constructed and verified. After screening ~6000 compounds, an antibacterial agent Merbromin was identified as a potent and selective inhibitor of 3CLpro.

* Corresponding author. School of Pharmaceutical Sciences, Xiamen University, Xiang'an South Road, Xiang'an District, Xiamen, Fujian, 361102, China.
** Corresponding author. Department of Neuroscience, School of Medicine, Xiamen University, Xiang'an South Road, Xiang'an District, Xiamen, Fujian, 361102, China.
E-mail addresses: WangZX@xmu.edu.cn (Z. Wang), huzhou@xmu.edu.cn (H. Zhou).
[1] These authors contributed equally to this work.

https://doi.org/10.1016/j.bbrc.2021.12.108
0006-291X/

2. Materials and methods

2.1. Materials

Substrate of 3CLpro, MCA-AVLQ↓SGFR-Lys(Dnp)-Lys-NH_2, was synthesized by GL Biochem Ltd (Shanghai, China). Amine Coupling Kit (Product code: BR100050) and Series S Sensor Chip CM5 (Product code: BR100530) used for SPR assay were purchased from Cytiva Ltd (United Kingdom). Glutathione-Sepharose 4B column and thrombin were purchased from Amersham Pharmacia Biotech (Sweden). Isopropyl-β-d-thiogalactoside (IPTG), Proteinase K, Papain and Trypsin were purchased from BBI Life Sciences Corporation (Shanghai, China).

2.2. Enzyme activity assay

The hydrolytic activity of 3CLpro was detected by using substrate MCA-AVLQ↓SGFR-Lys(Dnp)-Lys-NH_2 [6,10,11]. Experiments were performed on an opti384-well plate (Black, PE) with 60 μL of assay buffer (50 mM HEPES, pH 7.5, 0.1 mg/mL BSA, and 0.01% Triton X-100). Substrate of 3CLpro was used for the detection of Proteinase K, Trypsin, Papain.

Enzyme concentration was initially designed to be 0.2 μM, and reaction was launched by rapidly adding substrate (final concentrations from 0 to 30 μM). After 3 min reaction, fluorometric hydrolysate was measured by Victor Nivo Microplate Reader (PE, USA) (excitation: 340 nm, emission: 405 nm). The enzyme activity of 3CLpro was represented by Michaelis constant K_M and Conversion rate constant K_{cat}, which were determined by nonlinear regression based on Michaelis-Menten equation (Eqn. (1)).

$$V = \frac{K_{cat}[E][S]}{K_M + [S]} \tag{1}$$

where $[E]$ and $[S]$ are the concentrations of enzyme and substrate, respectively, and V represents the initial hydrolysis rate of substrate. In view of the dimer is the active form of 3CLpro, the $[E]$ in the above equation was required to be corrected as the concentration of dimer $[D]$ as shown in the following equation (Eqn. (2)) [11,12].

$$V_{max} = K_{cat}[D] = K_{cat}\frac{K_D + 4C_t - \sqrt{K_D^2 + 8K_DC_t}}{8} \tag{2}$$

Herein, K_D represents the dissociation constant of the dimer to monomer, and is defined by $K_D = [M][M]/[D]$, of which $[M]$ and $[D]$ are the concentrations of the monomer and dimer, respectively. C_t is the total protein concentration of monomer and dimer, and is calculated from $C_t = [M] + 2[D]$. On the basis of the equation, a set of hydrolysis rates under the varying concentrations of 3CLpro (0.2–1.4 μM) and fixed concentration of substrate (30 μM) were measured. The concentration of substrate was more than 3 times of K_M in order to generate the V_{max} in the initial phase of reaction. The value of K_D was calculated by using the nonlinear regression according to the plot of V_{max} to C_t. IC_{50} was obtained according to the following logistic regression function [13,14], Eqn. (3):

$$y = A1 + \frac{A2 - A1}{1 + 10^{p\cdot[\log(IC50) - \log(x)]}} \tag{3}$$

where A1 is the inhibition rate without inhibitor, A2 is the ideal constant of complete inhibition, x is the concentration of the inhibitor, y is the inhibition rate, and p is the Hill factor.

2.3. Analysis of inhibition type

After 10 min incubation of 10 or 20 μM of Merbromin with 0.4 μM of 3CLpro in the assay buffer, hydrolysis reaction was triggered by rapid injection of equal volume of substrate solution (10–60 μM) and carried out at 37 °C for 3 min. The apparent K_M and K_{cat} in the absence or presence of Merbromin were first evaluated by Michaelis-Menten equation, and then precisely calculated by the equation of mixed model inhibition (Eqn. (4)) [15].

$$V = \frac{K_{cat}[E][S]}{K_M\left(1 + \frac{I_c}{K_i}\right) + [S]\left(1 + \frac{I_c}{Alpha \times K_i}\right)} \tag{4}$$

where *Alpha*, K_i and I_c represent the mixed constant, inhibition constant and concentration of inhibitor, respectively.

2.4. Isothermal titration calorimetry (ITC) assay

ITC assay was performed on an ITC200 (MicroCal) at 25 °C. HEPES buffer (10 mM, pH 7.4) with 2% DMSO was used as the reaction buffer. Initially, the solution of compound (2 mM) was preloaded on the syringe, and was then sequentially injected into the reaction chamber containing 40 μM of proteases (3CLpro, Proteinase K, Papain or Trypsin) by the automatic titration apparatus. Interval between each titration was set to 120 s to allow the heat signals back to baseline. Control assay was performed with the identical titration process except for the titrated buffer without proteases. All the experimental data were calibrated by subtracting the data of control, and the data fittings were executed on the commercial analysis software of ITC200.

2.5. Surface plasmon resonance (SPR) assay

SPR assay was performed on a BIAcore T200 machine (General Electric). 3CLpro protein (20 μg/mL) prepared in sodium acetate buffer (10 mM, pH 4.0) was immobilized on a CM5 chip with 16,000 RU by amino coupling method. Merbromin was diluted in the running buffer (10 mM HEPES pH 7.4, 0.1% P20, 50 mM NaCl, and 0.25% DMSO). The kinetics assay was launched by the injection of Merbromin solution with a series of concentrations from 1.56 μM to 25.0 μM at a flow rate of 30 μL/min for 120 s. The association and dissociation were kept on monitoring for 300 s after the injection. Data was analyzed with the Heterogeneous Ligand Fitting of kinetic mode in the software of the BIAcore T200.

2.6. Fluorescence titration assay

The fluorescence titration was performed on an Eclipse fluorescence spectrophotometer (Varian). The excitation wavelength was set to 280 nm and the emission wavelengths were set between 290 and 480 nm. Protein solution (1.0 μM, 2 mL) prepared in HEPES buffer (10 mM, pH 7.4) was disposed by a continuous injection of Merbromin, with the final ratios of Merbromin to protein from 1 to 12. Data were analyzed according to the previous report [16].

2.7. Molecular docking study

Molecular docking studies of the binding between Merbromin and 3CLpro were performed by using the Molecular Operating Environment (MOE) software. Compounds were prepared according to partial charge, energy minimization, and geometry optimization before simulate docking. The 3D structure of 3CLpro (pdb 6m2n) downloaded from the Research Collaboratory for Structural Bioinformatics Protein Data Bank (RCSB PDB) was processed by "ignore waters", "build hydrogens" and "protonate 3D" under the condition of pH of 7.0 and salt value of 0.1. Two docking regions consisting of the catalytic area and junction of dimer were

predicted by the "site finder" procedure before docking. Docking process was launched by "dock" procedure with "induced fit" mode. Briefly, placement was set to "triangle matcher" mode, and london dG was used to rescoring. To gain more precision results, forcefield was also selected for refining, and affinity dG was used for rescoring. Finally, thirty docking poses were generated, and the best docking was selected as an outcome.

3. Results

3.1. Construction of the in vitro proteolytic activity model of 3CLpro

The procaryotic expression plasmid of 3CLpro was constructed and transformed into *E.coli* BL21. As shown in Supplemental Fig. 1, the expression of GST-3CLpro fusion protein was highly induced by IPTG in *E.coli*. After purification by affinity chromatograph and cleavage by thrombin, 3CLpro protein with more than 95% purity was obtained.

In the enzyme reaction system containing 0.2 μM of 3CLpro and 0–30 μM of substrate, the hydrolysis rate of 3CLpro at low substrate concentrations increased almost in a linear fashion with increasing substrate concentration, but gradually reached to a steady-state at very high substrate concentrations, exhibiting a typical Michaelis-Menten (MM) curve (Fig. 1A). Through the nonlinear fitting procedure based on MM equation, the enzymatic K_M and K_{cat} were determined to be 8.9 ± 0.8 μM and 0.28 ± 0.04 min^{-1}, respectively.

It has been reported that the dimer rather than the monomer is the active form of 3CLpro [12,17]. We then determined the composition of 3CLpro dimer in our reaction system. The proteolytic activity was measured in the presence of 30 μM substrate and different concentrations of 3CLpro. As shown in Fig. 1B, the hydrolysis rates against the concentrations of 3CLpro exhibited an exponential growth trend in the initial series of concentrations, implying a monomer-to-dimer transition with increasing 3CLpro concentration. Scatter data was fitted based on Eqn. (2), yielding the K_D of the dimer-monomer equilibrium (0.23 ± 0.06 μM). By plugging the values of K_D and C_T back into Eqn. (2), the actual concentration of dimer was calculated to be 0.039 μM under the condition of 0.2 μM of 3CLpro, and the value of K_{cat} was subsequently revised to be 1.44 ± 0.21 min^{-1}.

3.2. High-throughput screening of 3CLpro inhibitors

The feasibility of the model used for the high-throughput screening (HTS) assay was determined by evaluating the signal to noise ratio (SNR) and the Z′ factor. A statistical analysis between the blank (negative) and 3CLpro (positive) groups was performed under the reaction condition of 0.2 μM of enzyme and 20 μM of substrate according to the previous report [6]. Our result showed that the model had a reproducible SNR of 9.1–12.5 and a feasible Z′ factor (0.62–0.9) [18], meeting the requirements for HTS assay (Supplemental Fig. 2A). The Z′ factor between the 3CLpro group and the group of 3CLpro with Ebselen, a reported inhibitor of 3CLpro [6], was 0.58–0.71, indicating that Ebselen can be used as a positive control for screening 3CLpro inhibitors in this assay [18,19]. Based on our above investigation and the previous report [6], the reaction condition of 0.2 μM of 3CLpro and 20 μM of substrate was chosen for the subsequent HTS experiment. After screening ~6000 compounds, we found 33 compounds as potential 3CLpro inhibitors with more than 95% inhibition rate at 16.7 μM (Supplemental Fig. 2B). Consistent with previous reports [6], Ebselen, Disulfiram, PX-12, Shikonin, Tideglusib and TDZD-8 were screened out, indicating the reliability of our HTS system.

3.3. Identification of Merbromin as a selective and mixed-type inhibitor of 3CLpro

Among the screened potential inhibitors, Merbromin as a clinic drug intrigued us, and its IC_{50} was determined to be 2.7 ± 0.17 μM (Fig. 2A), comparable to the reported IC_{50} of PX-12 (16.62 μM) and Shikonin (12.03 μM) [6]. However, Merbromin exhibited weak inhibiting effect on Papain with an IC_{50} of 8.03 μM, and no significant effects on Trypsin and Proteinase K with the estimated IC_{50} values more than 70 μM (Fig. 2B–D). Thus, Merbromin is of certain selectivity in inhibiting 3CLpro.

We further investigated the inhibition type of Merbromin. As shown from the scatterplots in Fig. 2E, the initial hydrolytic activity of 3CLpro under the varying concentrations of the substrate were significantly decreased by Merbromin in a dose-dependent manner. The data points of three groups (0, 5, 10 μM of Merbromin) were fitted with nonlinear fitting procedure based on MM equation. Both the apparent K_M and K_{cat} of 3CLpro were affected by Merbromin, of which the value of K_M increased from 9.02 ± 2.52 to 14.28 ± 8.83 μM and the value of K_{cat} decreased from 1.45 ± 0.21 to 0.63 ± 0.21 min^{-1}. This kind of change suggested a mixed inhibition mechanism. Data were subsequently refitted using Eqn. (4) with global evaluation, and the common K_M, K_{cat}, mixed constant (Alpha) and K_i were estimated as 9.93 ± 2.92 μM, 1.53 ± 0.23 min^{-1}, 3.77 ± 3.96, and 3.93 ± 1.41 μM, respectively.

3.4. Binding of Merbromin to 3CLpro

We further investigated the binding of Merbromin to 3CLpro by ITC assay. The ITC reaction exhibited an exothermic effect after each

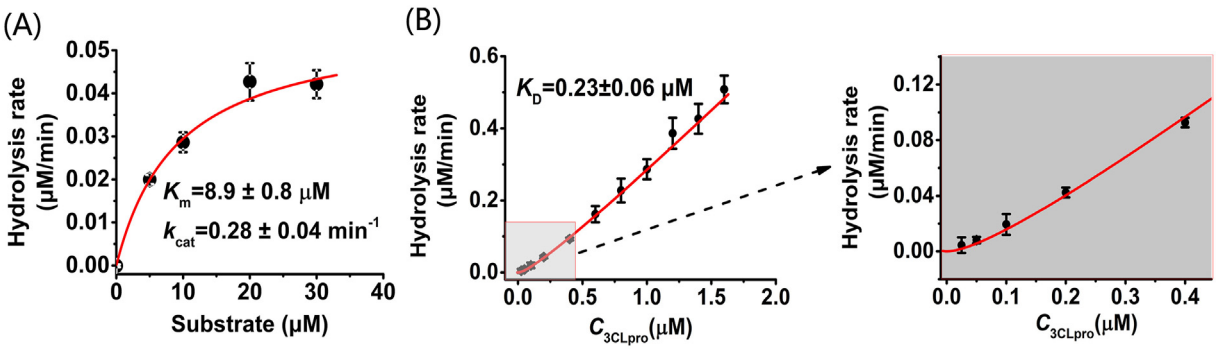

Fig. 1. Proteolytic activity of 3CLpro in vitro. (A) MM plot to show the hydrolysis rates of 3CLpro against the concentrations of substrate. (B) The kinetic response of 3CLpro activity to the concentrations of enzyme was plotted. The concentrations of 3CLpro were indicated and the substrate concentration was 20 μM. All data are shown as mean ± SD, n = 3 biological replicates.

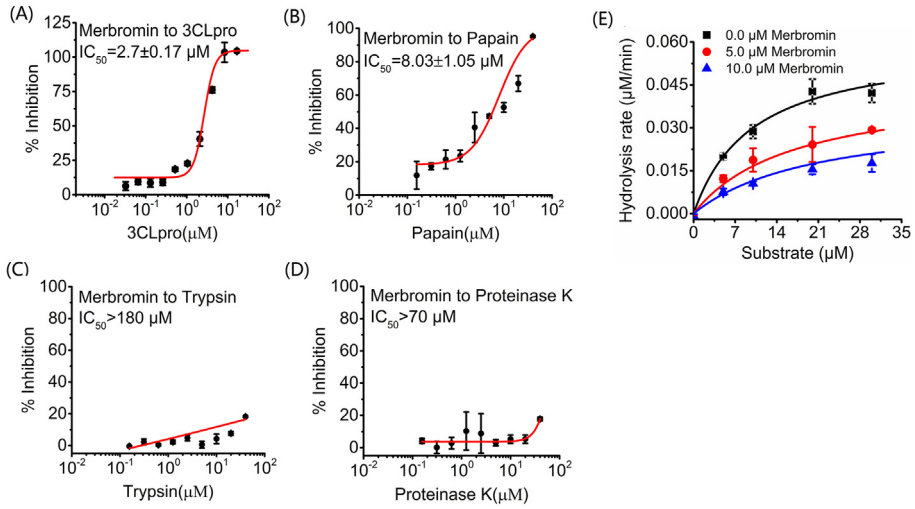

Fig. 2. Merbromin is a selective and mixed-type inhibitor of 3CLpro. (A–D) The hydrolytic activity of 3CLpro, Papain, Trypsin and Proteinase K were measured in the presence of different concentrations of Merbromin. (E) The hydrolysis rate of 3CLpro under increasing concentrations of substrate were detected in the absence and presence of 5 μM or 10 μM of Merbromin. All data are shown as mean ± SD, n = 3 biological replicates.

titration of Merbromin solution into the 3CLpro solution, of which a visible inflexion occurred in the titration when the ratio of Merbromin to 3CLpro was up to 3.7:1 (upper panel, Fig. 3A). This kind of thermal trend generally reflected the interaction between the two titrating molecules. The integral of each exothermic change against the ratio of Merbromin/3CLpro was plotted (lower panel, Fig. 3A). Interestingly, although the scatters presented a sigmoid type, they could not gain a suitable fitting by using traditional one-site binding model. We found that the exothermic change was not a simple decreasing process during the whole titration and it showed a slightly increasing tendency at the first five titrations. This implied that there were two binding sites of 3CLpro for Merbromin. Fitting results obtained by using "two sets of independent sites" model revealed that the dissociation constant K_D of the main binding between 3CLpro and Merbromin was 1.33 μM, while the K_D of the secondary binding was 67.8 μM. Besides, the thermodynamic process for Merbromin binding to both sites were negative enthalpies and positive entropy, implying that the main binding forces between 3CLpro and Merbromin were hydrogen bond and Van der Waals' interaction [20].

The binding kinetics were analyzed by Surface Plasmon Resonance (SPR) assay. As shown in Fig. 3B, Merbromin significantly increased the SPR response of 3CLpro in a dose-dependent manner. The R_{max} obtained from kinetic analysis reached up to approximate 600 RU that was 1.5 times of the theoretical R_{max} (420 RU), implicating the stoichiometric ratio of the binding between Merbromin

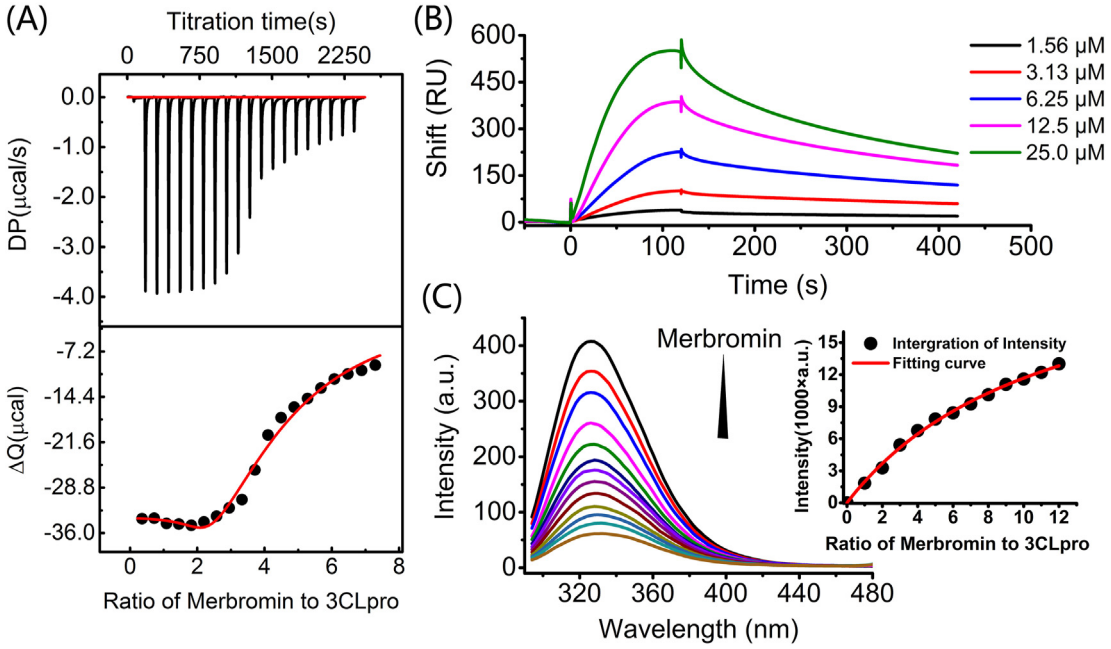

Fig. 3. Merbromin binds to 3CLpro. (A) ITC analysis of the binding of Merbromin to 3CLpro. Representative ITC data of the titration of Merbromin (2 mM) to 3CLpro (40 μM) in 10 mM HEPES buffer (pH = 7.4) was shown. The data of the peak area integrals for a series of titrations were fitted using the two sets of independent sites model. (B) SPR analysis of the binding of Merbromin to 3CLpro. (C) Fluorescence titration assay of Merbromin binding to 3CLpro. The fluorescence of 3CLpro was quenched by the successive titration of Merbromin with the ratio of Merbromin to 3CLpro from 1 to 12.

and 3CLpro might be more than "1", in accord with the result of our ITC assay. The kinetics of binding process was then evaluated by the heterogeneous ligand model to obtain two sets of binding parameters ($k_{a1} = 694.6 \pm 2.61$ L mol^{-1} s^{-1}, $k_{d1} = 1.25 \pm 0.01 \times 10^{-3}$ s^{-1}, $K_{D2} = 1.80 \pm 0.01$ μM, and $k_{a2} = 646.7 \pm 3.98$ L mol^{-1} s^{-1}, $k_{d2} = 16.25 \pm 0.08 \times 10^{-3}$ s^{-1}, $K_{D2} = 25.1 \pm 0.15$ μM).

The binding of Merbromin to 3CLpro was further confirmed by fluorescence titration assay (Fig. 3C). The endogenic fluorescence of 3CLpro could be dose-dependently quenched by Merbromin, implying the binding of Merbromin to 3CLpro. The data fitting procedure obtained an apparent K_D of 11.76 ± 0.98 μM, which fell in between the two K_D values of the two bindings obtained from either SPR or ITC assays.

We further evaluated the binding of Merbromin to three other proteases including Proteinase K, Papain and Trypsin whose activities were not significantly affected by Merbromin. The visible exothermic heat changes could be observed during the titration process for all the three proteases (Supplemental Figs. 3A–C), indicating the potential interactions between the three proteases and Merbromin since the dilution heat of Merbromin was endothermic (Supplemental Fig. 3D). However, these interactions, if existed, were extremely weak because no convergence of heat changing tendencies was observed under the same condition of Merbromin-3CLpro titration. The K_D of Merbromin to Proteinase K, Papain and Trypsin were roughly estimated to be 3 mM, 39 mM and 700 μM, respectively. Together, these results indicated that Merbromin selectively binds to 3CLpro.

3.5. Mimic docking of Merbromin to 3CLpro

To gain a further insight into the binding modes, the molecular docking simulation was performed (Fig. 4). As shown from the crystal structure (pdb:6m2n) [21], 3CLpro exists in a form of dimer (Fig. 4A). Several amino acid residues (Gly2, Phe3, Gly283, Arg4, Leu282, Lys5, Leu286, Glu288, Lys137, and Gly138) around the dimerization interface gathered by hydrogen bonds to form a pocket. This pocket was a potential binding site predicted by the "site finder" procedure of Molecular Operating Environment (MOE). Indeed, in our simulating docking, Merbromin bound to this site by forming hydrogen bonds with Glu288, Ser284 and Lys137 (Fig. 4C) and yielded the gliding energy of −6.68. This also suggested that Merbromin may regulate the formation of dimer to inhibit the activity of 3CLpro. In addition, Merbromin could also occupy the catalytic area with the gliding energy of −5.79. The sulfhydryl group of Cys145, a core residue in catalytic center, was forced to form hydrogen bonds with the carboxyl group of Merbromin (Fig. 4B). Besides, the pi-H bond formed between the benzene ring of Merbromin and the methylene of Glu166 further stabilized the binding. Thus, our docking study revealed the two binding sites in 3CLpro for Merbromin, consistent with the results obtained from our SPR and ITC binding assays.

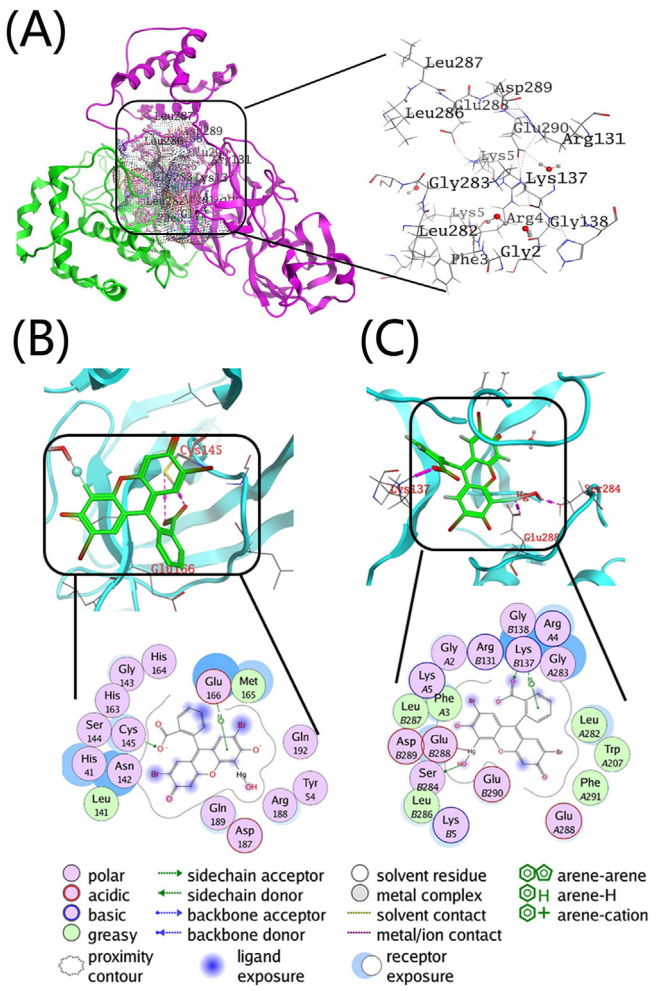

Fig. 4. The mimic model of the interaction between 3CLpro and Merbromin. (A) The 3D structure of 3CLpro dimer. A and B monomers are shown in green and violet, respectively. Dotted area around the dimerization interface was the potential binding site of 3CLpro. (B) The docking of Merbromin to the catalytic area of 3CLpro. (C) The docking of Merbromin to the dimerization interface. The amino acid residues of A and B monomer are annotated.

4. Discussion

COVID-19 caused by SARS-CoV-2 infection has become a serious public health issue in the world. Until now, no effective drugs are available for inhibiting SARS-CoV-2, and only some potential drugs including chloroquine and remdesivir were prudently recommended to clinical therapeutics [22–25]. Among the potential drug targets, 3CLpro has been extensively studied, due to its indispensable role in the maturity of function proteins during the virus replication process [4,26–28]. In this study, we constructed the in vitro screening model of 3CLpro and used it to screen ~6000 compounds by fluorescence-based HTS [9], leading to identifying Merbromin as a potent inhibitor of 3CLpro. Notably, Merbromin is of certain specificity in inhibiting 3CLpro, showing from its selectivity in inhibiting the proteolytic activity of 3CLpro and binding to 3CLpro.

Analysis of inhibition type based on enzymatic reaction showed that Merbromin was a mixed-type inhibitor of 3CLpro. Interestingly, binding data from both SPR and ITC assays suggested that 3CLpro possessed two sites for Merbromin binding. Consistently, molecular docking also revealed the two binding sites in 3CLpro. Merbromin could directly bind to the catalytic site of 3CLpro by forming hydrogen bond with Cys145, from which Merbromin directly inhibited the catalytic action of 3CLpro. Besides, Merbromin could also bind to the interaction interface formed by two monomers, by which Merbromin may function through modulating the dimer formation of 3CLpro. Thus, Merbromin binds to distinct sites of 3CLpro to employ two different mechanisms of inhibition, which may also render it as a mixed-type inhibitor of 3CLpro.

The structure of Merbromin contains mercury, which limits its usage due to the potential toxicity of mercury. However, it is worthwhile to trade-off the benefit of Merbromin on COVID-19 treatment and the risk of the side effects. Nevertheless, in view of its selective and potent effect on inhibiting 3CLpro, Merbromin can

serve well as a lead compound for the development of 3CLpro inhibitors with strong efficacy and low toxicity.

Author contributions

Conceptualization: XKZ, ZXW, and HZ; Data curation, Formal analysis and Funding acquisition: ZXW, and HZ; Investigation: JJC, YYZ, DQZ, BCZ, XHY, and ZPZ; Methodology: JJC, YYZ, and DQZ; Original draft: XKZ, ZXW, and HZ. All the authors approved the final version of the manuscript.

Declaration of competing interest

The authors declare that they have no known competing financial interests or personal relationships that could have appeared to influence the work reported in this paper.

Acknowledgements

We thank Professor Sheng-ce Tao (Shanghai Jiao Tong University, China) for kindly providing the DNA sequence of 3CLpro. This work was supported by the Fundamental Research Funds for the Central Universities [No. 20720200009], National Natural Science Foundation of China [Nos. 31770811, 32070779, and 82072777], and Fujian Province Science and Technology Major Special Project [No. 2021ZD02006].

Appendix A. Supplementary data

Supplementary data to this article can be found online at https://doi.org/10.1016/j.bbrc.2021.12.108.

References

[1] E. Aleebrahim-Dehkordi, et al., Human coronaviruses SARS-CoV, MERS-CoV, and SARS-CoV-2 in children, J. Pediatr. Nurs. 56 (2021) 70–79, https://doi.org/10.1016/j.pedn.2020.10.020.
[2] M. Kandeel, et al., From SARS and MERS CoVs to SARS-CoV-2: moving toward more biased codon usage in viral structural and nonstructural genes, J. Med. Virol. 92 (2020) 660–666, https://doi.org/10.1002/jmv.25754.
[3] S.N. Alharbi, A.F. Alrefaei, Comparison of the SARS-CoV-2 (2019-nCoV) M protein with its counterparts of SARS-CoV and MERS-CoV species, J. King Saud Univ. Sci. 33 (2021), 101335, https://doi.org/10.1016/j.jksus.2020.101335.
[4] J. Qiao, et al., SARS-CoV-2 M(pro) inhibitors with antiviral activity in a transgenic mouse model, Science 371 (2021) 1374–1378, https://doi.org/10.1126/science.abf1611.
[5] W. Zhu, et al., Identification of SARS-CoV-2 3CL protease inhibitors by a quantitative high-throughput screening, ACS Pharmacol Transl Sci 3 (2020) 1008–1016, https://doi.org/10.1021/acsptsci.0c00108.
[6] Z. Jin, et al., Structure of M(pro) from SARS-CoV-2 and discovery of its inhibitors, Nature 582 (2020) 289–293, https://doi.org/10.1038/s41586-020-2223-y.
[7] S. Yan, G. Wu, Potential 3-chymotrypsin-like cysteine protease cleavage sites in the coronavirus polyproteins pp1a and pp1ab and their possible relevance to COVID-19 vaccine and drug development, Faseb. J. 35 (2021), e21573, https://doi.org/10.1096/fj.202100280RR.
[8] E. Arutyunova, et al., N-terminal finger stabilizes the S1 pocket for the reversible feline drug GC376 in the SARS-CoV-2 M(pro) dimer, J. Mol. Biol. 433 (2021), 167003, https://doi.org/10.1016/j.jmb.2021.167003.
[9] T. Muramatsu, et al., SARS-CoV 3CL protease cleaves its C-terminal autoprocessing site by novel subsite cooperativity, Proc. Natl. Acad. Sci. U. S. A. 113 (2016) 12997–13002, https://doi.org/10.1073/pnas.1601327113.
[10] F. Wang, et al., Structure of main protease from human coronavirus NL63: insights for wide spectrum anti-coronavirus drug design, Sci. Rep. 6 (2016) 22677, https://doi.org/10.1038/srep22677.
[11] V. Grum-Tokars, et al., Evaluating the 3C-like protease activity of SARS-Coronavirus: recommendations for standardized assays for drug discovery, Virus Res. 133 (2008) 63–73, https://doi.org/10.1016/j.virusres.2007.02.015.
[12] S. Tomar, et al., Ligand-induced dimerization of Middle East respiratory syndrome (MERS) coronavirus nsp5 protease (3CLpro): IMPLICATIONS for nsp5 regulation and the development OF antivirals, J. Biol. Chem. 290 (2015) 19403–19422, https://doi.org/10.1074/jbc.M115.651463.
[13] P.G. Gottschalk, J.R. Dunn, The five-parameter logistic: a characterization and comparison with the four-parameter logistic, Anal. Biochem. 343 (2005) 54–65, https://doi.org/10.1016/j.ab.2005.04.035.
[14] D.A. Volpe, et al., Use of different parameters and equations for calculation of IC(5)(0) values in efflux assays: potential sources of variability in IC(5)(0) determination, AAPS J. 16 (2014) 172–180, https://doi.org/10.1208/s12248-013-9554-7.
[15] R.A. Copeland, Evaluation of enzyme inhibitors in drug discovery. A guide for medicinal chemists and pharmacologists, Methods Biochem. Anal. 46 (2005) 1–265. https://www.ncbi.nlm.nih.gov/pubmed/16350889.
[16] Z.X. Wang, et al., A novel spectroscopic titration method for determining the dissociation constant and stoichiometry of protein-ligand complex, Anal. Biochem. 206 (1992) 376–381, https://doi.org/10.1016/0003-2697(92)90381-g.
[17] S. De, et al., A monomer-dimer nanoswitch that mimics the working principle of the SARS-CoV 3CLpro enzyme controls copper-catalysed cyclopropanation, Dalton Trans. 43 (2014) 10977–10982, https://doi.org/10.1039/c4dt01508h.
[18] J.H. Zhang, et al., A simple statistical parameter for use in evaluation and validation of high throughput screening assays, J. Biomol. Screen 4 (1999) 67–73, https://doi.org/10.1177/108705719900400206.
[19] Y. Sui, Z. Wu, Alternative statistical parameter for high-throughput screening assay quality assessment, J. Biomol. Screen 12 (2007) 229–234, https://doi.org/10.1177/1087057106296498.
[20] P.D. Ross, S. Subramanian, Thermodynamics of protein association reactions: forces contributing to stability, Biochemistry 20 (1981) 3096–3102, https://doi.org/10.1021/bi00514a017.
[21] H.X. Su, et al., Anti-SARS-CoV-2 activities in vitro of Shuanghuanglian preparations and bioactive ingredients, Acta Pharmacol. Sin. 41 (2020) 1167–1177, https://doi.org/10.1038/s41401-020-0483-6.
[22] D. Camprubi, et al., Persistent replication of SARS-CoV-2 in a severely immunocompromised patient treated with several courses of remdesivir, Int. J. Infect. Dis. 104 (2021) 379–381, https://doi.org/10.1016/j.ijid.2020.12.050.
[23] M. Hoffmann, et al., Chloroquine does not inhibit infection of human lung cells with SARS-CoV-2, Nature 585 (2020) 588–590, https://doi.org/10.1038/s41586-020-2575-3.
[24] B.N. Williamson, et al., Clinical benefit of remdesivir in rhesus macaques infected with SARS-CoV-2, Nature 585 (2020) 273–276, https://doi.org/10.1038/s41586-020-2423-5.
[25] C. Wright, et al., Are hydroxychloroquine and chloroquine effective in the treatment of SARS-COV-2 (COVID-19)? Evid. Base Dent. 21 (2020) 64–65, https://doi.org/10.1038/s41432-020-0098-2.
[26] H.M. Froggatt, et al., Development of a fluorescence-based, high-throughput SARS-CoV-2 3CL(pro) reporter assay, J. Virol. 94 (2020), https://doi.org/10.1128/JVI.01265-20.
[27] W.S. Liu, et al., Screening potential FDA-approved inhibitors of the SARS-CoV-2 major protease 3CL(pro) through high-throughput virtual screening and molecular dynamics simulation, Aging (Albany NY) 13 (2021) 6258–6272, https://doi.org/10.18632/aging.202703.
[28] V. Mody, et al., Identification of 3-chymotrypsin like protease (3CLPro) inhibitors as potential anti-SARS-CoV-2 agents, Commun Biol 4 (2021) 93, https://doi.org/10.1038/s42003-020-01577-x.